Earthq Eng & Eng Vib (2009) 8:301-311 **DOI**: 10.1007/s11803-009-9018-3

Experimental investigation of damage behavior of RC frame members including non-seismically designed columns

Chen Linzhi†, Lu Xilin‡, Jiang Huanjun§ and Zheng Jianbo*

State Key Laboratory of Disaster Reduction in Civil Engineering, Tongji University, Shanghai 200092, China

Abstract: Reinforced concrete (RC) frame structures are one of the mostly common used structural systems, and their seismic performance is largely determined by the performance of columns and beams. This paper describes horizontal cyclic loading tests of ten column and three beam specimens, some of which were designed according to the current seismic design code and others were designed according to the early non-seismic Chinese design code, aiming at reporting the behavior of the damaged or collapsed RC frame strctures observed during the Wenchuan earthquake. The effects of axial load ratio, shear span ratio, and transverse and longitudinal reinforcement ratio on hysteresis behavior, ductility and damage progress were incorporated in the experimental study. Test results indicate that the non-seismically designed columns show premature shear failure, and yield larger maximum residual crack widths and more concrete spalling than the seismically designed columns. In addition, longitudinal steel reinforcement rebars were severely buckled. The axial load ratio and shear span ratio proved to be the most important factors affecting the ductility, crack opening width and closing ability, while the longitudinal reinforcement ratio had only a minor effect on column ductility, but exhibited more influence on beam ductility. Finally, the transverse reinforcement ratio did not influence the maximum residual crack width and closing ability of the seismically designed columns.

Keywords: reinforced concrete frame member; cyclic test; hysteresis behavior; damage behavior; seismic performance

1 Introduction

As one of the major natural disasters confronted by society, strong earthquakes often cause severe damage or even collapse of engineering structures, contributing to the loss of many lives and damage to properties. On May 12, 2008 at 14:28:01, the great Wenchuan earthquake, with magnitude 8 on the Richter scale, occurred in the Sichuan Province of southwestern China, resulting in tens of thousands of deaths and hundreds of billions RMB in losses (Xinhua Agency Net, 2008). Many school buildings, primarily reinforced concrete (RC) frame structures, were destroyed, and thousands of students lost their lives (Wang, 2008). These school buildings were constructed at different times, and some were designed according to seismic codes while others were not. This tragedy reminds the public again to seriously reconsider the seismic design of RC frame structures.

As generally accepted by the earthquake and structural engineering community, the performance based seismic design (PBSD) method provides a promising solution for the design of earthquake resistant engineering structures (SEAOC, 1995). The PBSD method allows structures to experience a certain level of damage during earthquakes, which necessitates the definition of damage levels that correspond to different performance objectives of structures. The performance of columns and beams is a key factor that influences the performance of the entire frame of a given structure. Therefore, in order to effectively control the damage levels of frame structures, it is important to investigate the earthquake-induced damage behavior of columns and beams. Low cycle cyclic tests are considered to be a powerful tool for studying the seismic performance of structural members, and have been frequently conducted by researchers throughout the world (Bae and Bayrak, 2008; Lukkunaprasit and Thepmangkorn, 2004). Among these tests, the overall observations reported most frequently were related to the hysteresis behavior and ductility of specimens. Although it is believed that cracking behavior, such as maximum crack width and residual crack width is closely related to the damage level and repair cost of RC members, cyclic tests with crack development observed throughout the entire testing process have rarely been reported in the literature. A series of spirally confined circular RC columns, often used in bridge piers, were tested by Lehman *et al*.

Correspondence to: Lu Xilin, State Key Laboratory of Disaster Reduction in Civil Engineering, Tongji University, 1239 Siping Road, Shanghai 200092, China
Tel: 86-21-65983430
E-mail: lxlst@tongji.edu.cn
†PhD Candidate; ‡Professor; §Associate Professor; * Master of Engineering

Supported by: National Natural Science Foundation Under Grant No. 50708081 and 90815029; Key Project of Chinese National Program for Fundamental Research and Development 2007CB714202; Innovation Program of Shanghai Municipal Education 09ZZ32
Received February 21, 2009; **Accepted** May 6, 2009

to study the effect of different design parameters on damage behavior under reversed cyclic loadings with low axial load ratios ranging from 0.10 to 0.20 (Lehman *et al.*, 2004). In Japan, considerable research efforts have been made in the post-earthquake assessment of RC framed buildings, using crack information as an important index for seismic evaluation (Maeda *et al.*, 2004). Furthermore, some of their achievements have been included in Guidelines for Post-Earthquake Damage Assessment and Rehabilitation of Reinforced Concrete Buildings (JBDPA, 2001). So far, there has not been much information available on these types of tests designed according to Chinese codes and considering the current practice of building construction in China.

Based on the damage and collapse behavior of RC frame structures observed during the Wenchuan Earthquake, 13 RC frame members were designed according to current seismic or early non-seismic Chinese design codes, representing different construction periods. The main design parameters include axial load ratio, shear-span ratio, and transverse and longitudinal reinforcement ratios. Horizontal cyclic loading tests were conducted, and the crack widths at peak drift and zero lateral force, i.e., the maximum crack width and residual crack width, respectively, were measured at each drift amplitude over the entire testing process. Through a careful test configuration, the compressive concrete strains at the edge of the specimen were derived based on the correspondingly measured displacements. Strains of transverse and longitudinal reinforcements and the height of concrete cover spalling were also measured. From a comprehensive analysis of the test results, some findings are presented concerning the effect of design parameters on damage behavior.

2 Experimental program

2.1 Specimen design

The design cubic concrete compressive strength was 30 MPa. All the column specimens had a square section with an edge length of 250 mm. All beams were rectangular with section 200 mm (width) × 400 mm (height). Concrete cover thickness was uniformly 25 mm. The axial load ratio was classified into four levels ranging from 0.1 to 0.7, where the axial load ratio (n) is defined according to Chinese seismic code (Ministry of Construction of China, 2002):

$$n = N/(f_c A_g) \tag{1}$$

in which N is the design axial load, A_g is gross section area, and f_c is the design value of concrete compressive strength:

$$f_c = 0.88 \times 0.76 \times \mu_{f_{cu}} / 1.4 \tag{2}$$

where $\mu_{f_{cu}}$ is the mean value of cubic compression strength of concrete specimens. Generally, the failure of members with a shear-span ratio L/h_0 larger than 3 in RC frame structures is often controlled by the structural flexural behavior. In this study, for all column and beam specimens, the shear-span ratio was larger than 3. For columns there were four volumetric transverse reinforcement ratios (ρ_v): 0.23%, 0.83%, 1.46% and 2.15%. The first one was lower than stipulated in the seismic code, which means that the corresponding specimen was not seismically designed. For beam specimens, two levels of area ratio of transverse reinforcement (ρ_s) were considered: 0.50% and 1.00%. As for longitudinal reinforcement ratio (ρ_l), two levels were assumed for the specimens. Characteristic values of concrete and steel rebar that were measured via material property tests are listed in Table 1 and Table 2, respectively. Typical design drawings are provided in Fig. 1, and detailed information for all the specimens is listed in Table 3.

2.2 Measurement and test procedure

Figure 2 illustrates the test set-up and measurement configuration along with a mechanical model of the test specimen. In order to monitor the concrete strains, four additional steel bars with a diameter of 10 mm were installed horizontally in the specimen at different levels within a region of 1.5 times the specimen section height measured from the specimen bottom. Each of these steel bars had a length equal to the specimen section height plus 2×100 mm so that it passed through the entire section and extruded 100 mm from each side of the specimen. Linear variable displacement transducers (LVDT) were mounted on these steel bars, enabling concrete strains in the above region to be derived from the measured relative displacements between the steel bars under the planar section assumption.

Table 1 Mean value of concrete properties MPa

Batch	Cubic strength	Prism strength	Modulus of elasticity
1	30.3	22.2	3.04×10^4
2	27.9	18.9	3.09×10^4

Table 2 Mean value of rebar strength

Diameter (mm)	Yield strength (MPa)	Ultimate strength (MPa)
10	338.3	488.3
14	355.0	520.0
16	350.0	506.7
22	335.0	500.0
25	391.5	555.6
6.5	423.3	463.3
8	408.3	481.7

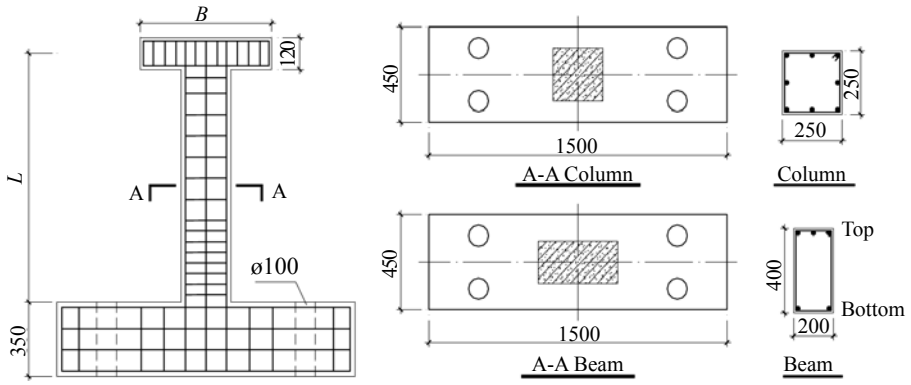

Fig. 1 Design drawings of specimens (dimensions in mm)

Table 3 Design parameters of specimens

Number	n	L/h_0	Hoops			Longitudinal		
			ρ_v (ρ_s) (%)	D (mm)	S (mm)	ρ_l (%)	N_{lr}	D (mm)
C301	0.1	3.4	1.46	6.5	40	1.97	8	14
C303	0.3	3.4	1.46	6.5	40	1.97	8	14
C305	0.5	3.4	1.46	6.5	40	1.97	8	14
C305L	0.5	3.4	1.46	6.5	40	1.00	8	10
C307	0.7	3.4	1.46	6.5	40	1.97	8	14
C505C	0.5	5.7	0.23	6.5	250	1.97	8	14
C505S	0.5	5.7	0.83	6.5	70	1.97	8	14
C505	0.5	5.7	1.46	6.5	40	1.97	8	14
C505D	0.5	5.7	2.15	8	40	1.97	8	14
C705	0.5	8.0	1.46	6.5	40	1.97	8	14
B22S	0.0	5.3	(0.50)	8	100	0.95 (Top) 0.50 (Bottom)	2 2	22 16
B25	0.0	5.3	(0.50)	8	100	1.94 (Top) 0.95 (Bottom)	3 2	25 22
B22	0.0	5.3	(1.00)	8	50	0.95 (Top) 0.50 (Bottom)	2 2	22 16

Notes: D is the diameter of steel rebar. S is the hoop spacing, and N_{lr} is the number of longitudinal rebar.

First, vertical load was applied to the fixed specimens and kept constant throughout the entire testing process. Then, horizontal load was applied by the actuator. Prior to the horizontal load reaching 75 percent of the predicted yielding force of the specimen, the test was controlled by the actuator force. As it approached the yielding force, control was transferred to displacement control. After the longitudinal rebar yielded, three cycles of loading and unloading were conducted for each displacement amplitude, increasing in multiples of specimen yielding displacement.

During the entire test process, the tip drift, horizontal force, longitudinal and transverse rebar strains and concrete crack width were measured. Maximum crack

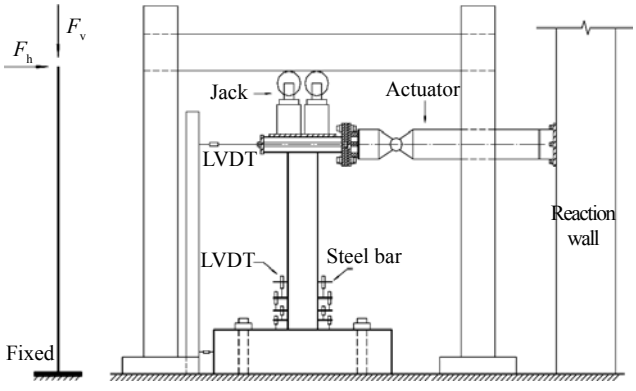

Fig. 2 Test set-up and arrangemnt of instruments

width and maximum residual crack width were measured at the peak horizontal force or displacement points and the zero-force points within each loading and unloading cycle, respectively. The instrument for measuring crack width has a range from 0.02 mm to 8 mm. When a crack first appeared its width was often less than 0.02 mm, thus only the crack distribution was recorded. The widths of cracks wider than 8 mm were estimated by using a steel ruler. Displacement of the anchoring beam at the bottom of each specimen, which was usually negligible, was also monitored by a displacement transducer, in order to derive the net drift of the specimen tip.

3 Test results

3.1 Overview

The sequence of damage according to the first occurrence was observed as follows: concrete cracking, yielding of the longitudinal rebar, initial spalling of the concrete cover, final spalling of the concrete cover, buckling of the longitudinal rebar and fracture of the longitudinal rebar. No fracture of hoops was found during any of the tests of the specimens. It was observed that flexural behavior dominated during tests of all specimens except column specimen C505C, which was designed according to the non-seismic code with hoop spacing of 250 mm. The crack width at first emergence was below 0.02 mm and spacing between cracks was approximately equal to the hoop spacing. Although the cracks became wider as the horizontal displacements increased, the maximum crack width during the second and third cycle was roughly the same as during the first cycle, and new cracks rarely emerged during repeated cycles of the same displacement amplitude. After yielding of the longitudinal rebar buckled, the concrete cover at the bottom of the specimens began spalling. The cover spalling continued until the longitudinal rebar buckled and crushed the concrete core. Typical flexural failure is shown in Fig. 3.

As reported recently, obvious shear damage was observed during the great Wenchuan Earthquake in RC frame structures designed according to early Chinese non-seismic codes. In these tests, the transverse reinforcement of specimen C505C was below the minimum requirement stipulated by the Chinese seismic design code (Ministry of Construction of China, 2002). The main diagonal crack appeared during the cycle with a displacement amplitude of 24 mm, and developed sharply. As illustrated in Fig. 4, as the main diagonal crack reached a width 15.5 mm, all longitudinal rebars buckled below the first stirrup away from the specimen bottom. The corner longitudinal rebars even buckled between the first and second stirrup from the bottom, indicating the weak confinement of the transverse reinforcement.

Compared to the symmetric damage on the opposite sides of the column specimens, damage to beam specimens was observed to be asymmetric, as shown in Fig. 5. Due to the fact that longitudinal reinforcement in the upper region of the beam specimen was about twice as much as in the bottom region, cover spalling first occurred on the weakly reinforced bottom region, as did the concrete core crushing. The concrete cover in the upper region, however, remained almost intact until the tests were finished. This is because when the upper region was in compression, the height of the compression region was fairly small, which was verified by the equilibrium of the vertical force acting on the beam section with great disparity of longitudinal reinforcement on two sides and no vertical load exerted. Therefore, the compressive concrete strains at the section edge did not reach an ultimate flexure value.

3.2 Hysteresis behavior

The hysteresis loops of some representative specimens are shown in Fig. 6, where major events are marked on the force-displacement curves. Table 4 lists the damage characteristics recorded for all specimens. Note that for specimens with relatively low axial load ratios, the horizontal force-displacement curves generally ascend during loading. However, as the axial

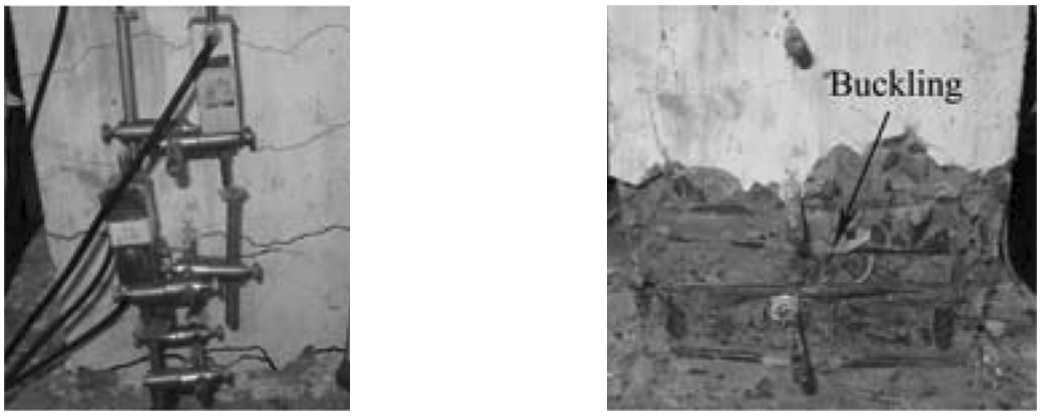

Fig. 3 Typical flexural failure of column specimens

(a) formation of diagonal crack (b) developing of diagonal crack

Fig. 4 Remarkable shear damage of column (C505C)

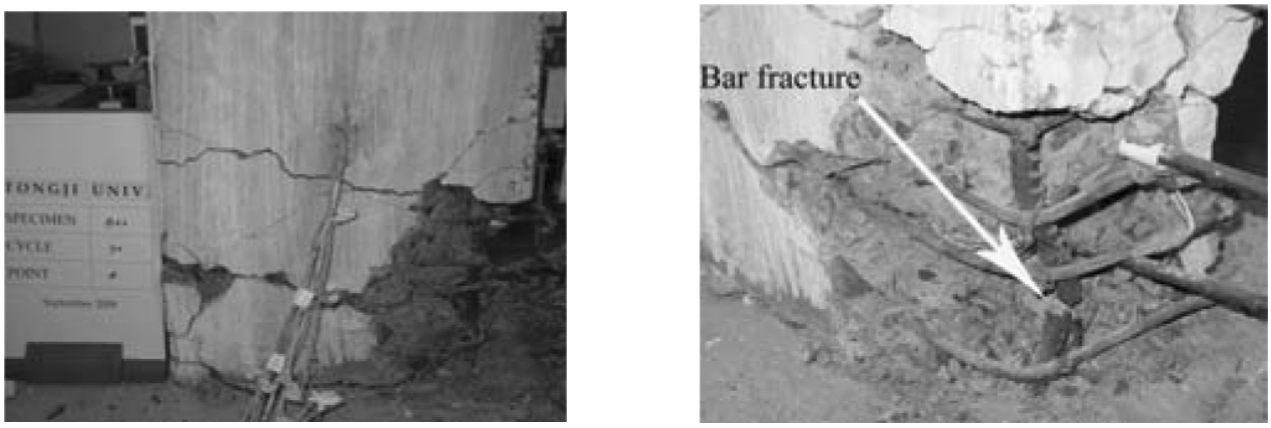

Fig. 5 Asymmetric damage behavior in beam specimens

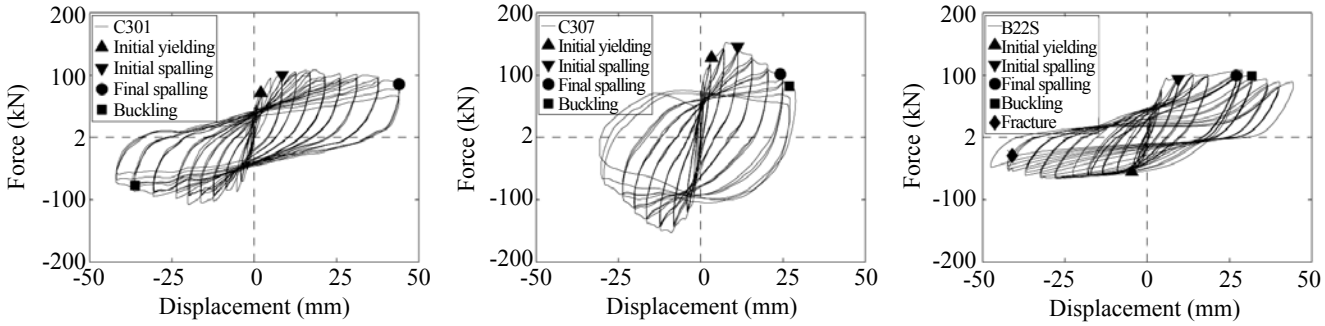

Fig. 6 Hysteresis of some specimens

load ratio increases, the horizontal force-displacement curve begins to drop down from the peak force point before it reaches its targeted displacement. Compared to the thickness of the hysteresis loops of the columns, the hysteresis of the beams exhibited some pinching behavior after final spalling of the concrete cover. Following the concrete core crushing of beams, the longitudinal rebar gradually lost the lateral support provided by the transverse reinforcement and began to buckle. The load carrying capacity of the beams remained at a relative high percentage until the longitudinal rebar fractured in the bottom region, when the hysteresis curves suddenly dropped and the tests were terminated.

Table 4 Damage characteristics recorded for all specimens

Specimen	Δ_y (mm)	Δ_{spall} (mm)	ε_{spall}	H_{spall} (mm)	H_{spall}/h	Δ_{buckle} (mm)	$\Delta_{fracture}$ (mm)
C301	2.02	8.52	-0.0075	170	0.68	36.13	Not found
C303	3.54	10.29	-0.0070	179	0.72	41.15	Not found
C305	3.00	9.94	-0.0072	196	0.78	29.14	Not found
C305L	2.17	6.30	-0.0101	189	0.76	Not found	Not found
C307	3.35	11.27	-0.0088	221	0.88	26.97	Not found
C505C	7.73	15.70	-0.0044	260	1.04	30.12	Not found
C505S	6.35	12.11	-0.0060	204	0.82	45.47	Not found
C505	12.75	31.11	-0.0043	240	0.96	62.41	Not found
C505D	9.55	19.64	-0.0073	148	0.59	54.88	Not found
C705	15.90	44.30	-0.0026	236	0.94	Not found	Not found
B22S	9.20	18.90	-0.0081	308	0.77	63.59	81.91
B25	9.35	31.75	-0.0053	383	0.96	97.61	Not found
B22	5.71	20.28	-0.0033	253	0.63	85.30	39.77
	Mean		-0.0063		0.81		
	COV		35%		17%		

Note: Δ_y, Δ_{spall}, Δ_{buckle} and $\Delta_{fracture}$ are the displacement at first yield of longitudinal rebar, initial cover spalling, buckling and fracture of longitudinal rebar, respectively. ε_{spall} is the concrete compressive strain at the specimen outer fiber at initial spalling of concrete cover. H_{spall} is the height of concrete cover spalling and h is section height of specimen.

3.3 Ductility evaluation

Ductility characterizes the capability of a structure or member to deform without significant degradation of its loading capacity, and is generally defined by the so-called ductility coefficient:

$$\mu = \Delta_u / \Delta_y \tag{3}$$

where Δ_u and Δ_y are the ultimate and yielding deformation, respectively. So far, there have been several methods for defining these two limit states (Bae and Bayrak, 2008; Park, 1989). Different definitions result in a remarkable difference in the ductility coefficient. Based on a sophisticated analysis of many results from similar laboratory tests on structures and members, Park concluded and indicated several definitions of ultimate and yielding deformation that can provide an estimate of the ductility coefficient that shows good agreement with test results (Park, 1989). In this paper, the yielding deformation was determined by the first yielding of the longitudinal reinforcement, or by the intersection of the horizontal line at maximum force with the straight line passing through the origin and the 75% maximum force point on the envelope curve, whichever was less. The ultimate state was defined by the point on the descending section of the envelope curve with a 15% force degradation (Ministry of Construction of China, 1997). For clarity, these definitions are illustrated in Fig. 7. The ductility of each specimen was computed for both the loading and unloading direction. And, their mean value was taken as the ductility of the specimen. Table 5 lists the ductility coefficients for all specimens.

Specimens are divided into several groups according to their axial load ratios, shear-span ratios and so on, so that all specimens in each group differ from each other by only one variable parameter. As shown in Fig.8, there were six groups available for the comparative investigation, among which four were for columns and two were for beams. In the axial load ratio group, the ductility coefficient decreased from 8.27 to 4.81 by 42 percent when the axial load ratio increased from 0.1 to 0.7, indicating that the axial load ratio has a significant effect on ductility. A similar situation was observed in the shear-span ratio group, which consists of specimens C305, C505 and C705 with L/h_0 of 3.4, 5.7 and 8.0, respectively. As the shear-span ratio increased from 3.4 to 8.0, the column ductility coefficient decreased from 6.46 to 3.53 with a 45 percent drop. Note that in the column volumetric transverse reinforcement ratio

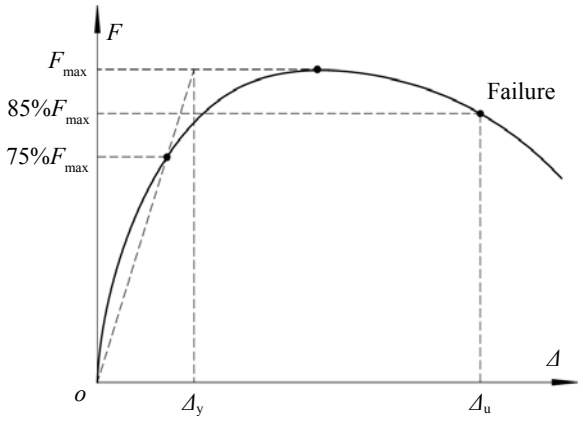

Fig. 7 Definition of yield and ultimate displacement

Table 5 Results of ductility coefficient

Specimen	Yielding displacement (mm)		Ultimate displacement (mm)		Ductility coefficient		
	Positive	Negative	Positive	Negative	Positive	Negative	Mean
C301	4.33	4.58	40.26	33.22	9.29	7.25	8.27
C303	4.72	3.10	30.71	27.86	6.51	8.99	7.75
C305	2.89	5.91	24.51	26.17	8.48	4.43	6.46
C307	3.08	4.13	16.19	17.97	5.26	4.35	4.81
C305L	3.55	3.49	25.79	24.51	7.26	7.02	7.14
C505C	7.78	7.75	27.22	25.05	3.50	3.23	3.37
C505S	7.99	5.93	30.28	33.53	3.79	5.65	4.72
C505	9.33	8.27	42.82	44.50	4.59	5.38	4.99
C505D	6.04	6.30	31.16	36.77	5.16	5.84	5.50
C705	12.47	12.53	51.58	36.62	4.14	2.92	3.53
B22	12.20	7.74	88.06	90.96	7.22	11.75	9.49
B22S	8.53	9.79	82.55	75.70	9.68	7.73	8.71
B25	18.38	9.62	91.50	65.56	4.98	6.81	5.90

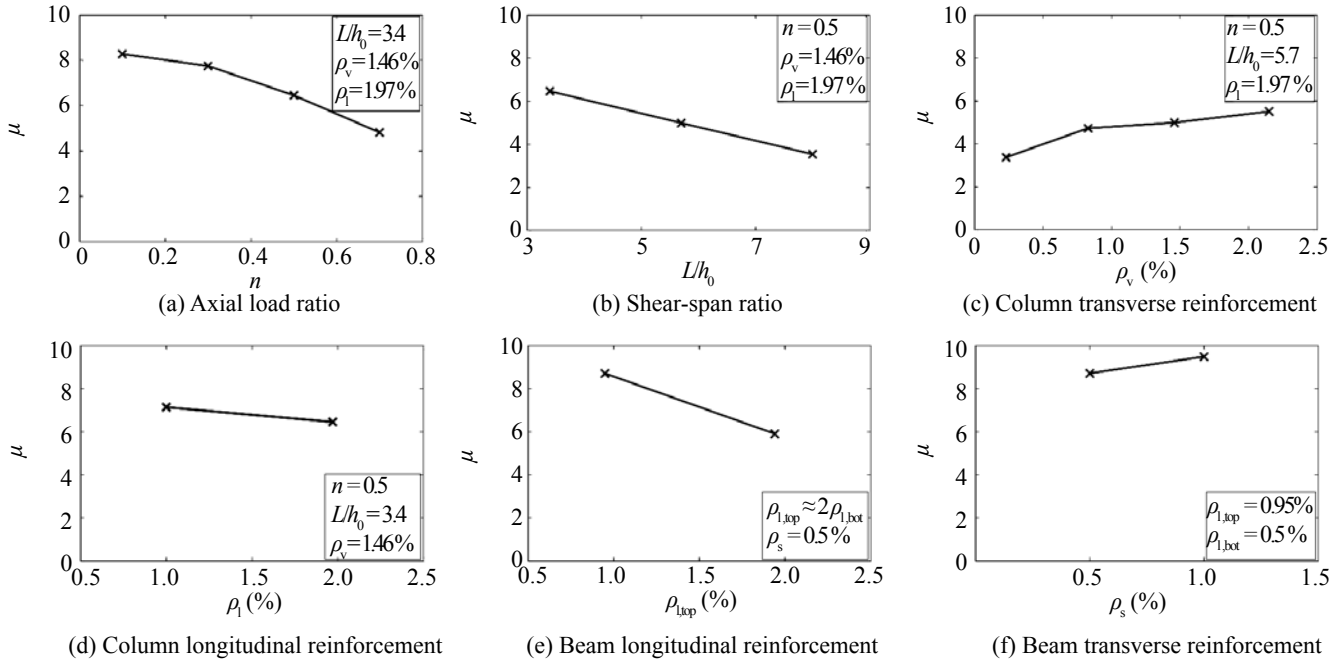

Fig. 8 Effect of different design parameters on specimen ductility coefficient

group, the non-seismically designed column yield had a lower ductility coefficient than the seismically-designed columns. For the seismically designed columns, the ductility coefficient increased from 4.72 to 5.50 by 16.5 percent as the transverse reinforcement ratio increased from 0.83% to 2.15%. A similar trend was observed for the area transverse reinforcement ratio group of beams. The longitudinal reinforcement ratio seemed to have a slight influence on the column ductility. The ductility coefficient decreased by 9.5 percent as the longitudinal reinforcement ratio increased from 1.00% to 1.97%. Since the longitudinal reinforcement in the upper region of the beam specimens was approximately twice that of the bottom region, the reinforcement ratio in the upper region was chosen as the abscissa. When the longitudinal reinforcement ratio in the upper region nearly doubled, the ductility coefficient decreased by 32 percent, demonstrating the pronounced effect of the longitudinal reinforcement ratio on beam ductility when compared to the columns.

3.4 Crack width

Crack width is accepted as an important index for evaluating the damage level of RC structures, and also serves as one of the decisive factors in

selecting appropriate retrofitting methods (Ministry of Construction of China, 2006). The maximum crack width and maximum residual crack width of all specimens, represented by w_m and $w_{m,res}$ respectively, are provided in relation to drift angle in Fig. 9 and Fig.10, respectively. The residual ratio of maximum crack width R_{mcw} is defined as the ratio of residual width to its maximum crack width. Figure 11 shows the relationship between R_{mcw} and drift for different design parameters.

Note that in a global sense, all the w_m, $w_{m,res}$ and R_{mcw} increase monotonically as the specimen drift angles increase. As illustrated in Fig. 9 and Fig. 10, the axial load ratio appears to be the most important factor for crack development. Both the maximum crack width and the maximum residual width decrease sharply as the axial load ratio increases, demonstrating the remarkable restraining effect of axial load on crack opening and its effect on promoting crack closing. Conceptually, the shear-span ratio presents a quantitative relationship between section moment and shear force. When the drift was less than 2%, w_m, and $w_{m,res}$ of specimens with shear-span ratios of 3.4, 5.7 and 8.0 were generally

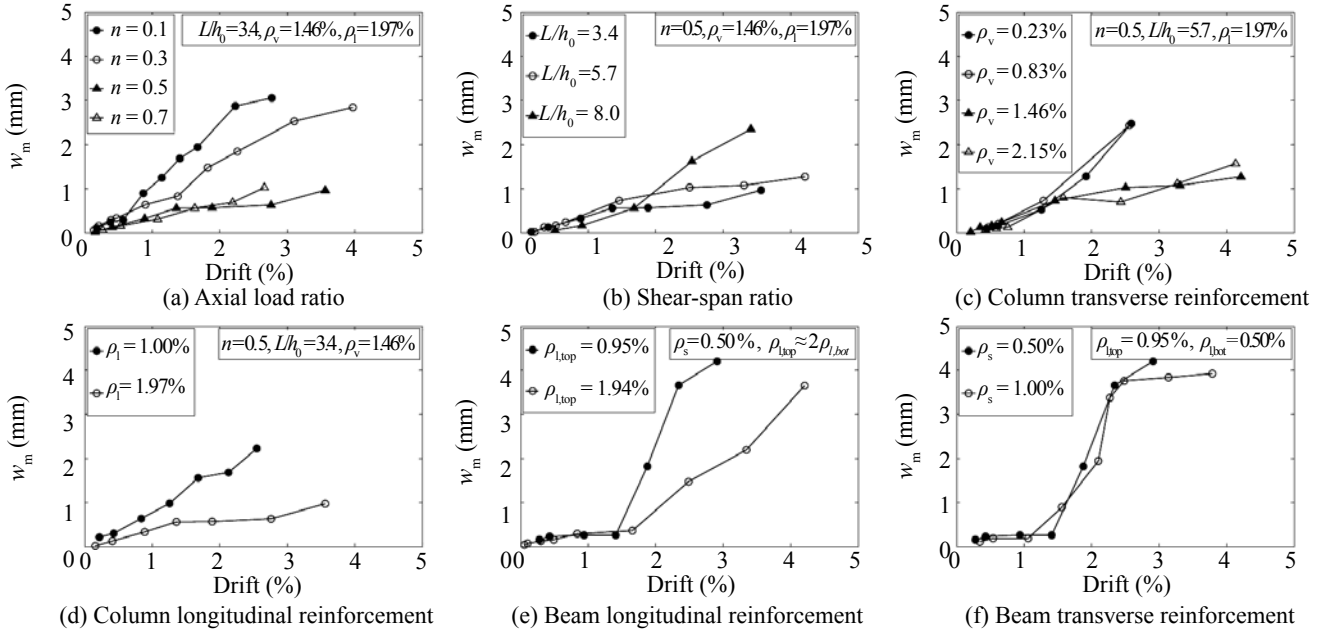

Fig. 9 Maximum crack width at peak drift

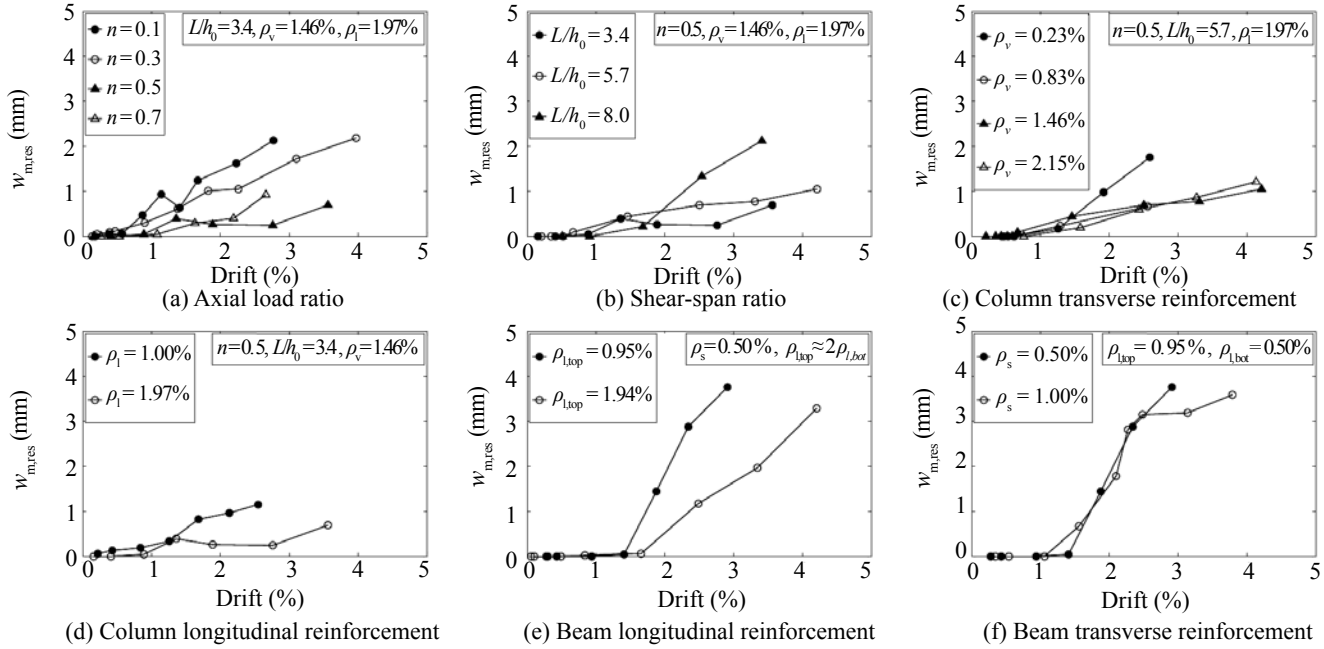

Fig. 10 Maximum residual crack width at zero lateral force

approximate to each other. For drift greater than 2%, cracks in specimens with larger shear-span ratios reached larger width during the loading process and remained larger when unloaded, implying the gradually increasing bending effect on columns. As for the group with a variable transverse reinforcement ratio, w_m of specimen C505S was much larger than specimens C505 and C505D, but near to C505C. This is explained as follows. Specimens C505C, C505S and C505 have the same hoop diameter of 6.5 mm (see Table 3). Their transverse reinforcement ratios were changed by the variation of hoop spacing. However, the hoop diameter of specimen C505D was 8 mm with the same spacing as specimen C505. Because of the weakening of the section brought by the hoops and the variation of bonding stress between the rebar and concrete, spacing of cracks often coincided with hoop spacing. It was generally accepted that larger spacing of cracks resulted in larger crack width; that is, sparse but wide cracks. This explains why the w_m of specimens C505 and C505D were approximate to each other and much less than for specimen C505S. Although hoop spacing in C505C was 3.6 times specimen C505S, new cracks formed between the existing ones as a result of the accumulation of bonding stress amounting to concrete tensile strength, which was why these two specimens yielded almost the same w_m. The $w_{m,res}$ of the seismically designed columns were very close to each other, but much less than in the non-seismically designed columns. When the drift was less than 2.5%, the area ratio of the beam transverse reinforcement was not significant on w_m and $w_{m,res}$. While the drift continued to increase, smaller values of w_m and $w_{m,res}$ were obtained for beams with denser hoops. The w_m and $w_{m,res}$ decreased as the longitudinal reinforcement ratio increased both in the column and beam specimens.

As shown in Fig. 11 and the corresponding damage characteristics shown in Table 4, most R_{mcw} curves ascended sharply after the longitudinal reinforcement yielded, and remained at high levels, suggesting the deterioration of crack closing capability caused by rapid accumulation of damage. The increase of the axial load ratio on the whole had a positive effect on crack closing. R_{mcw} gradually decreased as the axial load ratio increased from 0.1 to 0.5. The exception was that the R_{mcw} for an axial load ratio equal to 0.7 exceeded those for other axial load ratio values when drift was greater than 1%, which may result from the severe deterioration of restorability for lateral deformation due to the excessive axial load. The increase of the shear-span ratio had a negative effect on crack closing ability. No consistent relationship was found between R_{mcw} and the column transverse reinforcement ratio. Hence, the transverse reinforcement ratio did not seem to influence the crack closing ability of columns, although it affected w_m and $w_{m,res}$. This was also confirmed by the variation of R_{mcw} for beam specimens. The R_{mcw} of columns and beams were reduced by increasing the longitudinal reinforcement, indicating its positive influence on crack closing ability.

3.5 Cover spalling

Initial concrete cover spalling in these tests always appeared at 30 to 50 mm above the interface between the specimen and base stub, not just at the interface, demonstrating a constraining effect of the base stub in the intersection area. Based on the displacements measured in the lower region of the specimens, concrete

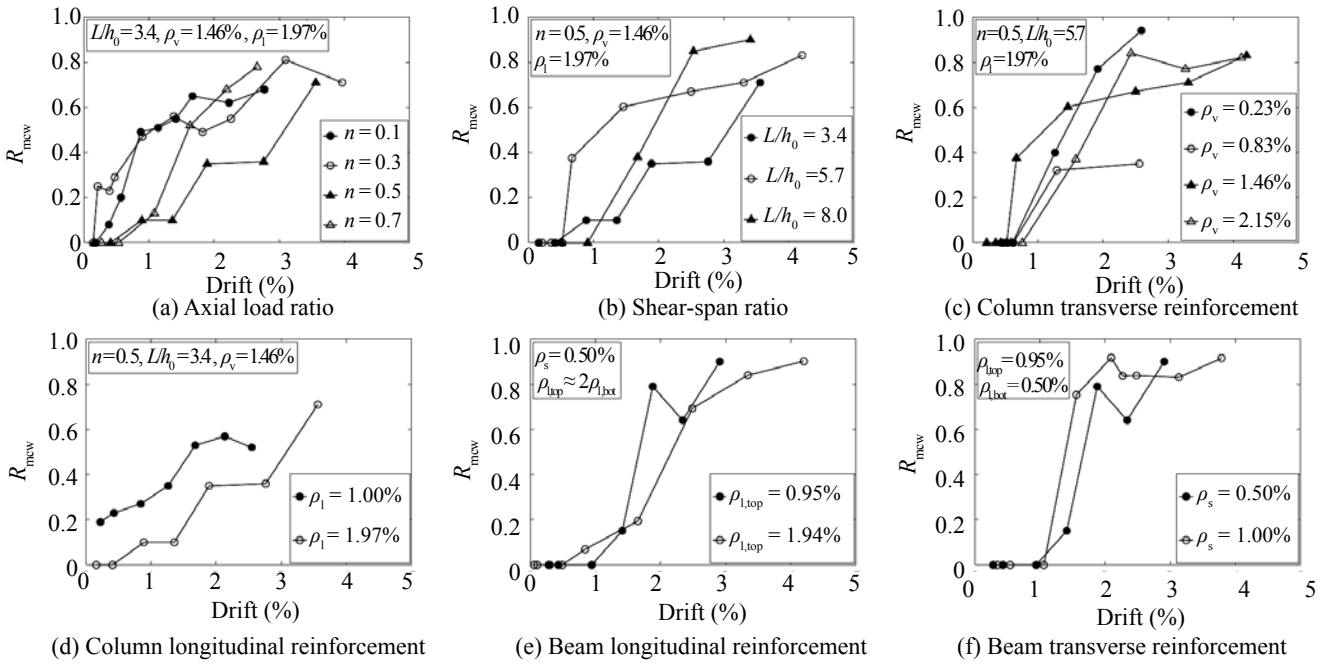

(a) Axial load ratio (b) Shear-span ratio (c) Column transverse reinforcement

(d) Column longitudinal reinforcement (e) Beam longitudinal reinforcement (f) Beam transverse reinforcement

Fig. 11 Residual coefficient of maximum crack width vs drift for different design parameters

strains were derived and their results are illustrated in Fig. 12. The compressive concrete strain ε_c at the outer fiber with a distance of c from LVDT2 can be obtained by the following equation:

$$\varepsilon_c = d_2 / l_2 \cdot (1 - c \cdot (d_1 / d_2 + 1) / l_1) \quad (4)$$

where d_1 and d_2 are the absolute value of relative displacements measured by LVDT1 and LVDT2, respectively. l_1 is the horizontal distance between LVDT1 and LVDT2, and l_2 is the height difference between the two steel bars.

Table 4 provides the concrete strains at initial cover spalling for all specimens with a minimum value of 0.0026 and maximum value of 0.0101. The mean value is 0.0063, and the coefficient of variation

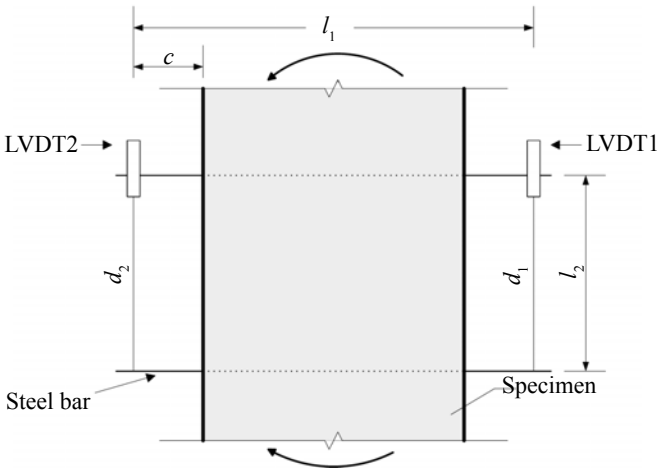

Fig. 12 Calculating concrete strain

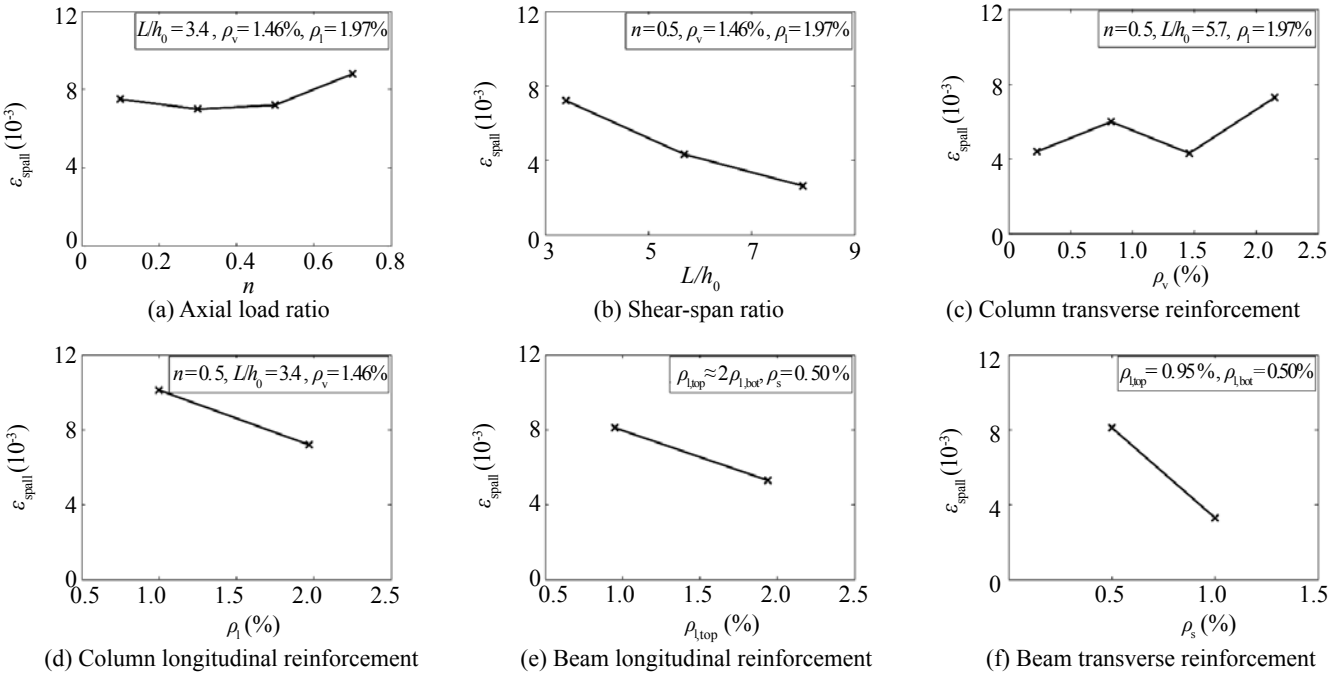

(a) Axial load ratio (b) Shear-span ratio (c) Column transverse reinforcement

(d) Column longitudinal reinforcement (e) Beam longitudinal reinforcement (f) Beam transverse reinforcement

Fig. 13 Effect of parameters on concrete compressive strain at initial cover spalling

(COV) is 35%. The effect of the design parameters on ε_{spall} is shown in Fig. 13. The shear-span ratio has the most pronounced effect on ε_{spall}, which drops by 64 percent when the shear-span ratio increased from 3.4 to 8.0. A remarkable effect was also observed for the column longitudinal reinforcement ratio, which was an increase of 97%, resulting in a decrease of 29% of ε_{spall}. A similar trend was found in the variation of beam longitudinal reinforcement. Specimens with axial load ratios of 0.1, 0.3 and 0.5 yielded similar values of ε_{spall}. But, the ε_{spall} for the specimen with axial load ratio of 0.7 increased about 20 percent. No consistent relationship was revealed between ε_{spall} and the transverse reinforcement ratios of columns and beams. Given the limited sample size, the large divergence of data and the inevitable influences from subjective judgment of initial cover spalling, more research is needed to further investigate these relationships.

The area of concrete cover spalling was closely related to the difficulty and cost of retrofitting. In this experimental study, the ratio of cover spalling height to section height ranged from 0.59 to 1.04, with a mean value of 0.81 and COV of 17%. Cover spalling height of the non-seismically designed specimen C505C reached 1.04 times the section height, implying extensive damage to members designed according to early non-seismic codes.

4 Conclusions

In this paper, thirteen RC frame members were designed according to current seismic or early non-seismic Chinese design codes based on the damage and collapse behavior of RC frame structures observed during the Wenchuan earthquake. Cyclic tests were conducted at the State Key Laboratory of Disaster Reduction in Civil Engineering, Tongji University. The following conclusions are drawn after comparative analysis of the test results.

(1) Premature shear failure was observed for the non-seismically designed column. Severe buckling of longitudinal rebar took place within a height of two times the section height away from the specimen base. The residual crack width and cover spalling height of the non-seismically designed column were much larger than for the seismically designed columns.

(2) The axial load ratio and shear-span ratio were the most important factors influencing column ductility. The longitudinal reinforcement ratio had a minor effect on column ductility, but exhibited a larger influence on beam ductility.

(3) The maximum crack width, maximum residual crack width and the ratio of residual width to the maximum crack width increased globally as the specimen drift increased. Severe deterioration of crack closing capability was found for most specimens after the yielding of longitudinal reinforcement, implying the rapid accumulation of damage. The axial load ratio seemed to be the most important factor affecting the crack opening and closing behavior. An increase in the axial load ratio can evidently reduce the maximum crack width and effectively promote crack closing when unloading. A decrease of shear-span ratio results in a restraining effect on crack opening and promotes crack closing, as does an increase in the longitudinal reinforcement ratio. These effects existed for increased beams with transverse reinforcement only when the drift exceeded 2.5%. No consistent relationship was found between the transverse reinforcement ratio and cracking behavior for seismically designed columns.

Acknowledgement

The financial support from the National Natural Science Foundation of China under Grants No. 50708081 and 90815029, Key Project of Chinese National Program for Fundamental Research and Development 2007CB714202, and Innovation Program of Shanghai Municipal Education 09ZZ32, are gratefully acknowledged.

References

Bae S and Bayrak O (2008), "Seismic Performance of Full-scale Reinforced Concrete Columns," *ACI Structural Journal*, **105**(2): 123–133.

Japan Building Disaster Prevention Association (JBDPA) (2001), *Guideline for Post-earthquake Damage Assessment and Rehabilitation of Reinforced Concrete Buildings*.

Lehman D, Moehle J, Mahin S, Calderone A and Henry L (2004), "Experimental Evaluation of the Seismic Performance of Reinforced Concrete Bridge Columns," *Journal of Structural Engineering*, **130**(6): 869–879.

Lukkunaprasit P and Thepmangkorn J (2004), "Load History Effect on Cyclic Behavior of Reinforced Concrete Tied Columns," *Journal of Structural Engineering*, **130**(10): 1629–1633.

Maeda M, Nakano Y and Lee KS (2004), "Post-earthquake Damage Evaluation for R/C Buildings," *Proceedings of the CTBUH 2004 Seoul Conference*, Seoul, Korea, 371–377.

Ministry of Construction of China (1997), *Specification for Methods of Seismic Testing of Buildings (JGJ 101-96)*, Ministry of Construction of China, Beijing. (in Chinese)

Ministry of Construction of China (2002), *Code for Seismic Design of Buildings*, Beijing: China Architecture & Building Press. (in Chinese)

Ministry of Construction of China (2006), *Design Code for Strengthening Concrete Structure (GB50367-2006)*, Beijing: China Architecture & Building Press. (in Chinese)

Park R (1989), "Evaluation of Ductility of Structures and Structural Assemblages from Laboratory Testing," *Bulletin of the New Zealand National Society for Earthquake Engineering*, **22**(3): 155–166.

SEAOC (1995), *Performance Based Seismic Engineering of Buildings*, Vision 2000 Committee, Structural Engineers Association of California, Sacramento, California.

Wang Z (2008), "A Preliminary Report on the Great Wenchuan Earthquake," *Earthquake Engineering and Engineering Vibration*, **7**(2): 225–234.

Xinhua Agency Net (2008). "Progress of Post-quake Relief and Reconstruction for the Great Wenchuan Earthquake," from http://news.xinhuanet.com/politics/2008-08/12/content_9197042.htm. (in Chinese)